行政院國家科學委員會專題研究計畫 期中進度報告

半導體表面奈米導線化學(1/3)

計畫類別：個別型計畫
計畫編號：NSC91-2113-M-002-036-
執行期間：91 年 08 月 01 日至 92 年 07 月 31 日
執行單位：國立臺灣大學化學系暨研究所

計畫主持人：張哲政

報告類型：精簡報告
報告附件：出席國際會議研究心得報告及發表論文
處理方式：本計畫可公開查詢

中 華 民 國 92 年 6 月 2 日

行政院國家科學委員會專題研究計畫成果報告

半導體表面奈米導線化學 (1/3)

Nanowire Chemistry on Semiconductor Surfaces

計畫編號： NSC 91-2113-M-002-036

執行期限： 91 年 8 月 1 日至 94 年 7 月 31 日

主持人： 張哲政

執行機構及單位：臺灣大學化學系

Abstract

Nickel nanoparticles were grown on oxide-covered silicon substrates by thin film deposition using metal vapor deposition and thermal treatment to specific temperatures. The nanoparticle growth process was characterized by X-ray photoelectron spectroscopy, Auger electron spectroscopy, scanning electron microscopy, scanning Auger microscopy, and atomic force microscopy. The silicon substrate was used as received, after ultrasonic cleaning in the de-ionized water, or pretreated by incubation under a mixing atmosphere of Ar and oxygen to produce a SiO_2 layer of 10-nm thickness. It was followed by a controlled growth of Ni films in the reducing environment of hydrogen via exposure to a Ni metal vapor source. On the Ni/SiO_2/Si surface, Ni nanoparticles of various sizes were evolved by thermal treatment to different substrate temperatures in the hydrogen environment. The shape and the size of the nanoparticles evolved depend on the substrate temperature, the starting Ni film thickness, and the heating time. Ni nanoparticles of ~19 nm diameter were produced on the SiO2 surface from the Ni film of 1 nm thickness by heating the substrate at 700 ℃ for 30 min. In contrast, few nanoparticles were formed on the Ni/native oxide/Si surface treated thermally. Nickel, instead of aggregates, diffuses into the native oxide layer to form the mosaic film of Ni patches on the silicon substrate. It suggests that the interaction of Ni atoms with the native oxide surface was sufficiently strong to prevent the formation of isotropic nanoparticles upon heating. X-ray photoelectron spectroscopic studies showed that, after thermal treatment, Ni was present on the Ni/native oxide/Si surface mainly in the chemical form of oxide, while that on the Ni/SiO_2/Si surface in the metallic state.

Key Words: nanoparticles, chemical vapor deposition, carbon nanotubes, nickel aggregates, agglomeration, thin film

Introduction

The potential of using nanostructures in reduced dimensions as the building blocks of future nanoscale electronic devices and the opportunity of creating and tailoring novel nanostructures have propelled the nanoscience to become one of the most promising areas of science for materials of next generation. The success in the last few years in tailoring nanoparticles in the semiconductor or insulator host further opens up new possibilities to fabricate innovative materials and devices for applications in many fields, including biomaterials[1] and optoelectronics.[2,3] According to the identity, the composition, and the size of the nanoparticles as well as the mean distance between them and the system temperature, the optical, electrical, and transport properties of the materials can be strongly modified.[4-13] A large positive magnetoresistance effect was also observed in weak magnetic fields from granular Fe/SiO_2 films within the compositional range corresponding to insulators.[14] The nature of the effect was attributed to the influence of ferromagnetic cluster aggregates of iron nanoparticles on the magnetoresistance.

In addition, metal nanoparticles stabilized on silica exhibits remarkably high catalytic activity.[15] The Pd/SiO_2 nanocatalyst has shown remarkably high activity for the catalytic hydrogenation of 2-hexanone, cyclohexanone, benzonitrile, cyclohexene, and benzene.[15] Catalytic complexes supported on non-porous nanoparticles also exhibits higher olefin hydroformylation as compared to the catalysts with conventional porous granular-SiO_2 support.[16] Nanoparticles of heteronuclear

complexes trapped in oxides may be used as recyclable catalysts for selective isomerization, selective dimerization, and hydrogenation and hydrogenolysis of alkenes as well as for efficient catalytic reduction of the aromatic C-C bonds.[17]

The metal nanoparticles that exhibit unusual reactivities are either supported, embedded, encapsulated on oxides.[17] They may be prepared either by the ion-beam method,[11,13] sol-gel process,[18] liquid phase deposition method,[12] pulsed laser deposition,[19] or by chemical reduction of an organometallic precursor.[15,20] Furthermore, metal clusters and nanoparticles, with controllable particle size, may be efficiently assembled in the solid matrix by incorporation in the matrix different types of oxides and by varying the molar ratio of the oxides to better manage the reducibility of the metal ions.[21]

These approaches for fabricating nanostructures, however, are not only complicated and costly, but also associated with intrinsic difficulties. For example, studies have concluded that the unique properties of the nanoparticles embedded by the ion-beam method in oxides may be related to the presence of strong compressive stresses acting on the particles which are caused by the surrounding glass matrix.[22]

This study was conducted in part to develop a simple and convenient synthesis method that could fabricate on the oxide surface nanoparticles with lateral dimensions as small as ~20 nm. The synthesis approach proceeded by depositing thin films of metals using a metal vapor source, followed by a controlled annealing process. Production of nickel nanoparticles on SiO_2 surfaces was realized in this work because of its well-known applications in the catalytic growth of carbon nanotubes via chemical vapor deposition of organic gases as the carbon source. Numerous papers have reported interesting electrical, thermal and mechanical properties[23-27] associated with carbon nanotubes. The role of nickel in the growth of CNT was also explored so as to understand if the exact features of CNT synthesized may be strategically altered by controlling experimental parameters related to nickel.

Experimental

Layers of Ni nanoparticles were synthesized on silicon oxide films grown on silicon wafer substrates of Si(100). In the synthesis, the wafer substrates were immersed in about 5% hydrofluoric acid solution for 30 min and then cleaned with the distilled water. A layer of SiO_2 was then incubated on the Si(100) substrate in an oven which had been purged with Ar gas before addition of oxygen gas. The incubation was conducted at 850 ℃ for one hour under a mixing atmosphere of Ar and oxygen. During this period, the pressure ratio of Ar to oxygen gas in the oven was maintained at 1:3. The SiO_2/Si sample was then allowed to cool down slowly to room temperature in the Ar atmosphere. The property of the sample was verified by AES and XPS.

Ni films of 1-20 nm were then prepared on the oxide films by deposition from a Ni metal vapor source which was made of the W wire on which short Ni threads were wounded. During the preparation, the working pressure of the chamber was kept in the range of 10^{-5}-10^{-8} torr. The W wire was resistively heated to 1000–1200 ℃ to maintain a large Ni/W atom ratio at the contacts so as to avoid the formation of their low-melting-point eutectic phase. The SiO_2/Si sample was placed at 5 cm away from the Ni threads and the sample temperature was maintained at room temperature. The thickness of the Ni film deposited was controlled by varying the exposure time of the Si(100) substrate to Ni vapor and determined using the quartz balance and angle resolved XPS (model VG Scientific ESCALAB 250).

To produce layers of Ni nanoparticles, the Ni films obtained were thermally treated in a vacuum system consisting of a quartz glass tube and a tube furnace. After the substrates covered with Ni films were introduced into the furnace, the reactor was first evacuated to less than 10^{-6} torr using a turbomolecular pump and then purged by argon twice before hydrogen was introduced to flow through. The substrates were then heated in the furnace to a specific synthetic temperature in the reducing environment of hydrogen, with the hydrogen gas pressure maintained at ~10 torr. The synthesis temperature was in the range of 550-850 ℃. Unless specified otherwise, the heating time of the

substrates lasted for 30 minutes. At the end of the thermal treatment, the samples were furnace-cooled slowly in the hydrogen environment.

The morphologies of the samples were examined using scanning electron microscopy (SEM), scanning Auger microscopy (SAM) and atomic force microscopy (AFM). Both SEM and SAM studies were performed using VG Scientific Microlab 350 while AFM was conducted on Digital Instruments DI 5000, which provides images with a lateral resolution of 2 nm and a depth resolution of 0.01 nm. All the microscopic images were obtained at room temperature. Using a filed emission gun (FEG) as the electron source, the SEM images were collected with 512 x 512 image pixels and the SAM images were collected with 128x128 image pixels. The FEG beam voltage was set at 10 or 25 kV during the acquisition of SEM images and the electrical current measured at the sample was 2.0 nA. The acquisition time per image was 8 sec. A longer acquisition time of about 4-8 hours was required for obtaining SAM images of acceptable S/N ratios. A lower FEG voltage at 10 kV and a smaller target current at 0.9 nA were thus employed when SAM images were taken.

Results and Discussion

3-1 Silica Film

The silicon oxide film prepared on the silicon wafer substrate was analyzed to ensure that the Ni film deposited subsequently was on a thin silicon oxide film of good purity. Shown in Fig. 1 is the Auger spectrum taken from the silicon dioxide surface prepared by exposing the cleaned silicon wafer in air at 850 ℃ for one hour, followed by cycles of Ar+ ion bombardment and annealing. The spectrum shows peak signals at kinetic energies of 80, 510, and 1612 eV. The signals observed at 80 and 1612 eV resulted from secondary electrons emitting via the Auger LMM and KLL transitions, respectively, from silicon on the sample surface. The one measured at 510 eV was due to the electrons emitting via the Auger KLL process from oxygen on the surface. Calculations by taking relative sensitivity factors of 0.5 and 0.022,[28] respectively, for these peaks showed that the surface concentration of oxygen atoms was ~8%.

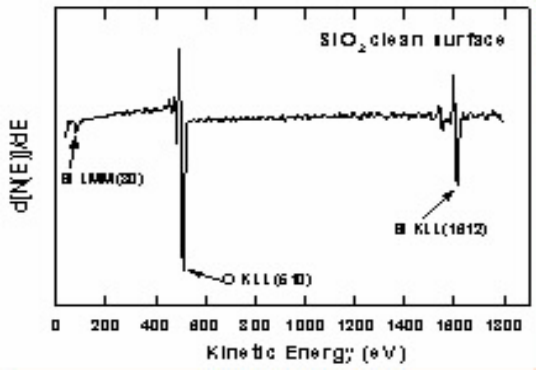

Figure 1.Auger electron spectrum obtained from the surface of the silicon dioxide film prepared

The thickness of the oxide film prepared was determined using angle resolved XPS. As shown in Fig. 2, the XPS spectrum taken at 0° from normal emergence of photoelectrons has peaks at ~99.1 eV from the elemental Si of the wafer substrate and a peak at 103.6 eV from the oxidized Si of the oxide film. The area of the peak obtained at 103.6 eV is considerably larger than the one measured at ~99.1 eV, indicating that, as predicted, the substrate was covered with oxides. The ratio of these two peaks became even larger when measurements were taken at higher angles of 20° and 40° from the surface normal. At the grazing angle of 60° from the normal, the substrate signal disappeared, which indicates that the thickness of the oxide film was ~10 nm.

Figure 2. XPS spectra measured from the silica/Si surface at the indicated take-off angles.

3-2 Nickel/Silica Film

3-2-1 Film thickness

The silicon oxide films were then used as the substrates on which Ni were deposited. A previous report on the preparation and characterization of Au/SiO2 films has shown that the size and shape of Au nanoparticles produced may be controlled by varying the thickness of the Au layer prepared in a multi-target magnetron sputtering system.[29] The Ni film morphology induced by annealing the Ni films of various thicknesses deposited on silicon oxide was examined. Presented in Fig. 3 are SEM images obtained from the Ni/silicon oxide sample surfaces after the samples were heated at 700 C in the hydrogen atmosphere for 30 min. As shown in the

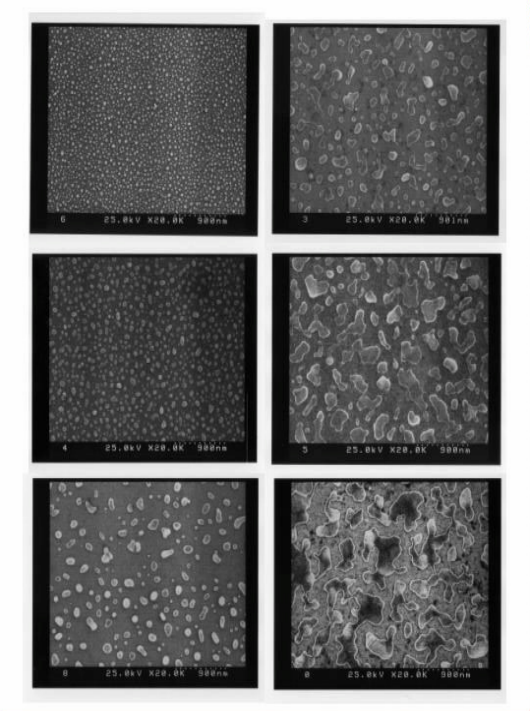

Figure 3. SEM Images taken from SiO2/Si surfaces covered by Ni thin films of (left from top)1nm, 2.5nm, 7.5nm, (right from top)10nm, 15nm, and 20nm thickness.

figure, the Ni film deposited on silicon oxide was metamorphosed during heating into flecks and aggregates. Small flecks appeared in the SEM images taken on the 1-nm Ni/SiO_2 film after the film was annealed. The size of the flecks was similar and they were about 19 nm in diameter. These nanofeatures were mostly in the round or oval shape. As the film thickness was increased, the size of the aggregates produced on the annealed sample surface was also increased. The average size, calculated as half of the sum of the length and the width of the aggregate, was 30 nm in diameter for

the 2.5-nm Ni film, 90 nm for the 7.5-nm film, and 400 nm for the 20-nm film. Surface structures with dimensions in the nanometer scale can thus be produced by heating the Ni/silica film at high temperature. In addition, there was a larger distribution in size and in shape of the aggregates after heating when a thicker Ni film was deposited on silica. The number density of the aggregates formed on silica, however, decreased with the film thickness.

Information on the topographic corrugation of the sample surface produced was obtained using atomic force microscopy (AFM). Fig. 4 compares the AFM images taken from the sample surface before and after Ni deposition and annealing. Figs.

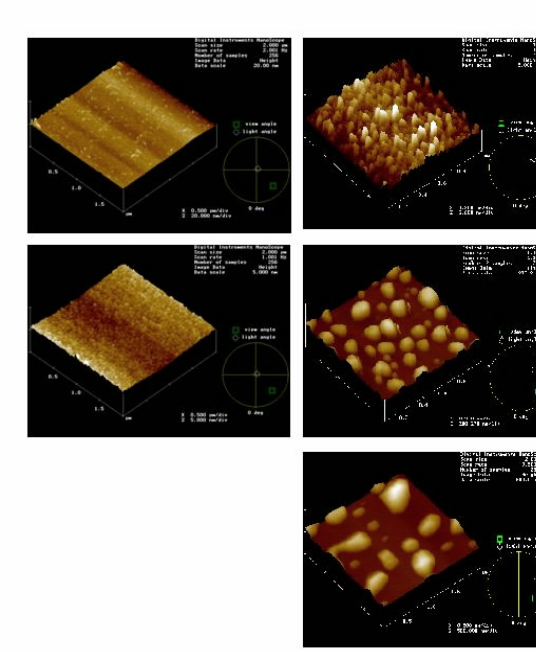

Figure 4. AFM images obtained from (left top) the SiO2/Si surface, (left middle) the 7-nm NI/SiO2/Si surface, and (right from top) SiO2/Si surfaces covered by 2nm, 7nm, and 20 nm Ni films followed by annealing at 700 C for 30 min. .

4a and 4b display the images obtained on the SiO_2 film before Ni deposition and on the 7-nm Ni/SiO_2 film before annealing. The images shown in Figs. 4c, 4d, 4e, all taken after the sample heating at 700 C in a hydrogen atmosphere of 10 torr for 30 min, were obtained on the 2.5-nm Ni/SiO_2 film, the 7-nm Ni/SiO_2 film, and the 20-nm Ni/SiO_2 film. As shown in the figure, both the SiO_2 film and the 7-nm Ni/SiO_2 film exhibited a high degree of surface smoothness before annealing, with a topographic corrugation of less than 1 nm. Three-dimensional features protruding from the silica surface were distinctively revealed in the AFM images after the Ni/silica film was annealed. The corrugation increased to 30 nm and 200 nm for the the 2.5-nm Ni/SiO_2 film and the 20-nm Ni/SiO_2 film, respectively. Granular aggregates in the nanometer scale were thus formed on the heated sample surface from the thin Ni film deposited on silica, with larger granules produced from the thicker film.

The chemical composition of the thermally treated, Ni despoited silica surface was examined using scanning tunneling microscope (SAM). Because the information depth of Auger electrons is less than a few nanometers, SAM can better map the chemical composition of surfaces than EDX and RBS. SAM also offers a better image resolution, in the ten-nanometer range, than the imaging methods employing x-rays as the probe. Presented in Fig. 5

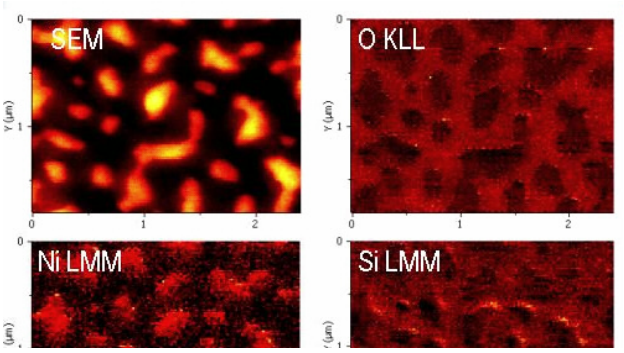

Figure 5. SEM and SAM images taken from the 20-nm Ni/SiO2/Si surface.

includes a SEM image taken from the 20-nm Ni/SiO_2 film, after it is thermally treated at 700 C in a hydrogen atmosphere of 10 torr for 30 min, and SAM images taken from the identical area of the surface as the SEM image. As discussed before, the SEM image revealed a distribution in size of aggregate features with irregular shapes on the annealed film surface. The corresponding Ni SAM image, measured by collecting electrons emitted from the surface with kinetic energies at the Ni LMM Auger peak of 846 eV, indicated that nickel mainly existed in the aggregate features (bright areas) shown in the SEM image, although small signals of Ni were also detected in other portion of the film surface.

In addition, SAM images made of O KLL Auger signals collected at 506 eV and of Si LMM signals measured at 1614 eV were also taken. The O SAM image showed that oxygen was predominantly present on the annealed film surface in the region away from the aggregate features. Even though the Si SAM image obtained had a poor signal-to-noise ratio, possibly because of low Auger yields in the high kinetic energy range of emitted electrons, after data collection of 8 hours, it also revealed that the spatial distribution of Si on the annealed Ni/silica film was in complement to that of nickel and in consistent with that of oxygen. Nickel on the aggregates was thus mainly in the metallic state, instead of in the chemical state of oxide or silicide. It also indicated that the dark area observed in the SEM image consisted of silicon oxide. The metallic nickel distribution on the anneal Ni/silica film surface thus corresponds well to the brightness of the spots observed in the SEM image. Heating the Ni/silica film in the hydrogen environment at 700 C thus caused nickel in the deposited film to conglomerate into metallic nanoparticles, leaving a portion of the silica substrate to be exposed. The change in the shape of the Ni nanoparticle with the thickness of the deposited film indicated that there may be a critical surface tension for Ni atoms conglomerating on silica, above which the tension breaks down and aggregates of irregular shape were formed.

3-2.2 Substrate Temperature

The effect of the substrate temperature upon the formation of Ni nanoparticles on silica was investigated. Presented in Fig. 6 are SEM images taken from a 20-nm Ni/silica film after the film was thermally treated at the indicated temperature in a hydrogen atmosphere of 10 torr for 30 min. As shown in the figure, a substrate temperature of 550 C was not high enough to cause Ni on the silica film to transform completely to nanoparticular aggregates. However, the Ni film deposited on silica already cracked with some areas of the silica underneath exposed. Heating the substrate to a temperature of 650 C caused Ni islands, though mostly interconnected, of irregular shapes started to appear. More silica underneath was exposed, with Ni islands breaking apart from their interconnections to form individual aggregates, as the substrate temperature was raised to 750 C. Both the number density and the degree of irregularity in shape of Ni aggregates were decreased when the Ni/silica film was annealed to 850C.

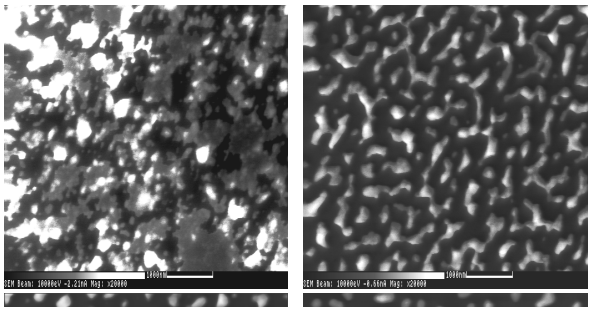

Figure 6. SEM images taken after the 20-nm Ni/SiO2/Si surfaces were thermally treated in the hydrogen environment of 10-torr pressure at 550 C (top left), 650 C (top right), 750 C (bottom left) and 850 C (bottom right) for 30 min.

Fig. 7 shows SEM images taken under the same experimental conditions as the ones used to obtain Fig. 6, except that the thickness of the Ni film deposited was 7 nm, instead. The figure shows that the interconnection between Ni islands broke at lower substrate temperature for the 7-nm Ni film than for the 20-nm film. Comparing the state of the Ni film transformed to at the same substrate temperature, it shows that the sample covered with the thinner Ni film reached a better uniformity in the shape of the granules formed at a lower substrate temperature than the thicker one. The number density of Ni nanoparticles formed was lower and the average size smaller for the silica film deposited with the thinner Ni film than the thicker one, as pointed out from Fig. 3 before.

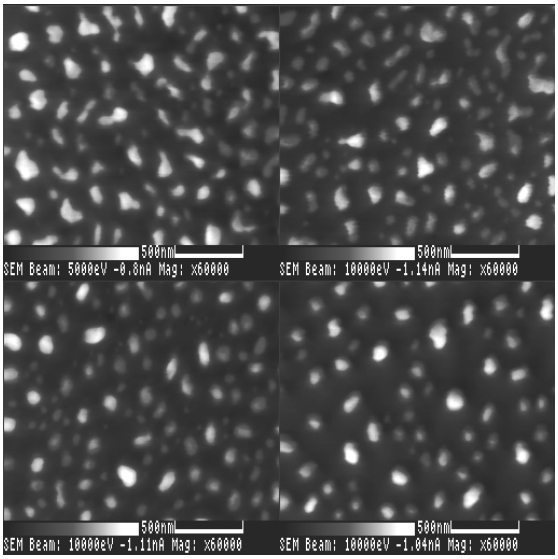

Figure 7. SEM images taken after the 7-nm Ni/SiO2/Si surfaces were thermally treated in the hydrogen environment of 10-torr pressure at 550 C (top left), 650 C (top right), 750 C (bottom left) and 850 C (bottom right) for 30 min.

3-2.3 Annealing Time

Figs. 8 and 9 show the effect of the length of the heating time on the morphology of the Ni/silica film surface. Nanoparticles of Ni were produced

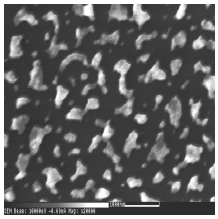

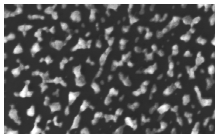

Figure 8. SEM images taken after the 20-nm Ni/SiO2/Si surfaces were thermally treated in the hydrogen environment of 10-torr pressure at 750 C for 5 min (top), 10 min (middle), and 40 min (bottom).

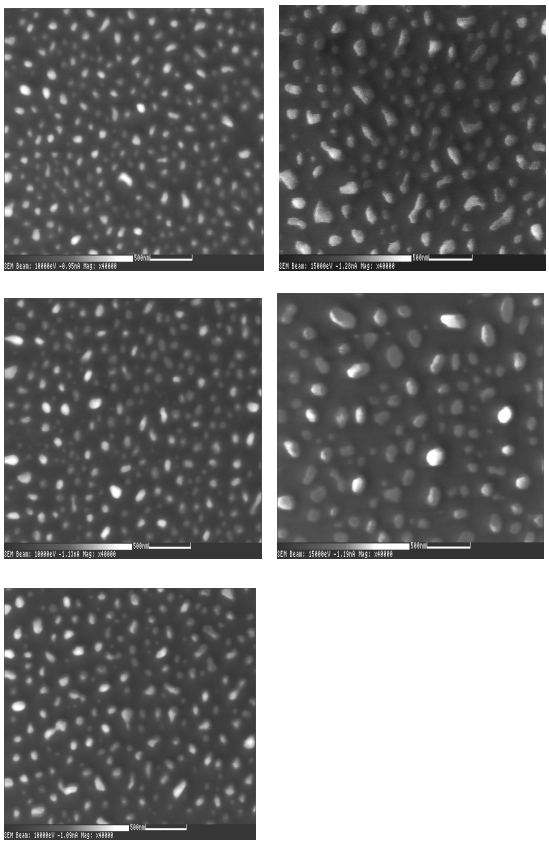

Figure 9. SEM images taken after the 7-nm Ni/SiO2/Si surfaces were thermally treated in the hydrogen environment of 10-torr pressure at 750 C for 5 min (top left), 10 min (middle left), 30 min (bottom left), 40 mon (top right), and 60 min (middle right).

on the 7-nm Ni/silica film surface after the substrate was annealed to 750 C in the hydrogen environment for 5 min. Increasing the substrate temperature did not significantly alter the morphology of the surface, except that the size of the nanoparticles was increased with time and the number density of the nanoparticles decreased. On this film surface, nanoparticles aggregate in an extended period of heating to form larger granules. The average particle size increased by a factor of ~2.5 in diameter as the heating time was increased from 5 min to 60 min.

Heating the 20-nm Ni/silica film in the hydrogen environment for 5 min at 750 C, however, caused the film to crack apart extensively (Fig. 8a), as compared with the image (Fig. 6a) obtained at 550 C for 30 min. Increasing the heating time led to the break down of the interconnection among Ni islands. A large number of smaller islands were thus formed. Similar to the temperature effect on the film morphology, an extended period of heating to 40 min also caused the transformation of islands on the film surface to nanoparticles of less irregularity.

3-3 Nickel/Native Oxide Film

Thermal treatment thus causes Ni on the silica surface to aggregate and the Ni film deposited is transformed during high-temperature heating and/or an extended period of substrate annealing into a distribution in size of nanoparticles. It is interesting to know if the Ni film deposited on the native oxide film of silicon behaves similarly. The study was carried out on the native oxide film of 5 Å – 20 Å thickness which was formed on the Si(100) surface exposed to air. Presented in Fig. 10 are SEM

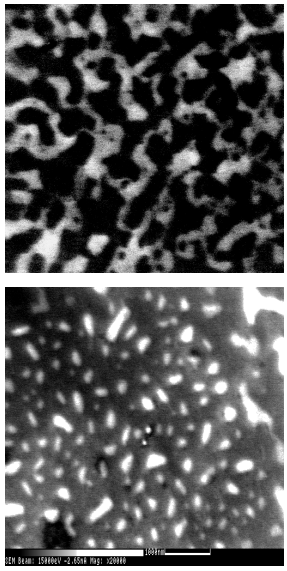

Figure 10. SEM images taken after the 7-nm Ni/native oxide/Si surfaces were thermally treated in the hydrogen environment of 10-torr pressure for 30 min at 700 C (top) and at 850 C (bottom)..

images of the 7-nm Ni/native oxide film which was annealed at 750 C and 850 C, respectively, in the hydrogen environment for 30 min. As shown in the figure, bright areas, with dimensions of a few hundred nanometers to more than one micron in length, were observed on the dark background. Tilting the sample did not cause the appearance of shadows on the sides of the bright areas away from the incident electron beam. It indicated that the variation in brightness of the areas observed in Fig. 10a did not result from a difference in height of the structural features present on the film surface.

References

1. Trapalis CC, Kokkoris M, Perdikakis G, Kordas G. *J. Sol-Gel Sci. Technol.* **2003**, 26, 1213.
2. Lin CF, Chung PF, Chen MJ, Su WF. *Optics Lett.* **2002**, 27, 713.
3. Zhang JY, Ye YH, Tan XL. *Appl. Phys. Lett.* **1999**, 74, 2459.
4. Bera SK, Chaudhuri S, Pal AK. *J. Phys. D* **2000**, 33, 2320.
5. Mulvaney P, Liz-Marzan LM, Giersig M, Ung T. *J. Mater. Chem.* **2000**, 10, 1259.
6. Selvan ST, Hayakawa T, Nogami M, Kobayashi Y, Liz-Marzan LM, Hamanaka Y, Nakamura A. *J. Phys. Chem. B* **2002**, 106, 10157.
7. Morita M, Kajiyama S, Rau D, Sakurai T, Iwamura M. *J. Lumines.* **2003**, 102, 608.
8. Ung T, Liz-Marzan LM, Mulvaney P. *J. Phys. Chem. B* **2001**, 105, 3441.

9. Kishimoto N, Takeda Y, Umeda N, Gritsyna VT, Lee CG, Saito T. *Nucl. Instrum. Meth. Phys. Res. Sec. B* **2000**, 166, 840.

10. Johansson P. *Phys. Rev. B* **2001**, 64, 165405.

11. Stepanov AL, Hole DE, Townsend PD. *J. Non-Crystal. Solids* **1999**, 244, 275.

12. Deki S, Ko HYY, Fujita T, Akamatsu K, Mizuhata M, Kajinami A. *Euro. Phys. J. D.* **2001**, 16, 325.

13. Lopez R, Haynes TE, Boatner LA, Feldman LC, Haglund RF. *Optics Lett.* **2002**, 27, 1327.

14. Varfolomeev AE, Sedova MV. *Phys. Solid State* **2003**, 45, 529.

15. Dominguez-Quintero O, Martinez S, Henriquez Y, D'Ornelas L, Krentzien H, Osuna J. *J. Molec. Catal. A* **2003**, 197, 185.

16. Li ZH, Peng QR, Yuan YZ. A*ppl. Catal. A* **2003**, 239, 79.

17. Blum J, Gelman F, Abu-Reziq R, Miloslavski I, Schumann H, Avnir D. *Polyhedron* **2000**, 19, 509.

18. Abe K, Sanada Y, Morimoto T. *J. Sol-Gel Sci. Technol.* **2001**, 22, 151.

19. Guczi L, Horvath D, Paszti Z, Toth L, Horvath ZE, Karacs A, Peto G. *J. Phys. Chem. B* **2000**, 104, 3183.

20. Yoo JW, Hathcock D, El-Sayed MA. *J. Phys. Chem. A* **2002**, 106, 2049.

21. Gurin VS, Petranovskii VP, Bogdanchikova NE. *Mater. Sci. Eng. C* **2002**, 19, 327.

22. Dubiel M, Hofmeister H, Schurig E, Wendler E, Wesch W. *Nucl. Instrum. Meth. Phys. Res. Sec. B* **2000**, 166, 871.

23. B. Q. Wei, R. Vajtai, P. M. Ajayan, *Appl. Phys. Lett.* **2001**, 79, 1172.

24. M. Kociak, A. Y. Kasumov, S. Gueron, B. Reulet, I. I. Khodos, Y. B. Gorbatov, V. T. Volkov, L. Vaccarini, H. Bouchiat, *Phys. Rev. Lett.* **2001**, 86, 2416.

25. J. W. Che, T. Cagin, W. A. Goddard, *Nanotechnology* **2000**, 11, 65.

26. P. Kim, L. Shi, A. Majumdar, P. L. McEuen, Phys. Rev. Lett. ***2001****, 87, 5502.*

27. M.-F. Yu, O. Lourie, M. J. Dyer, K. Moloni, T. F. Kelly, R. S. Ruoff, *Science* **2000**, 287, 637.

28. L. E. Davis, N. C. MacDonald, P. W. Palmberg, G. E. Riach, R. E. Weber, *"Handbook of Auger Electron Spectroscopy"*, Physical Electronics Industries, Inc., 1978.

29. Liao HB, Wen WJ, Wong GKL. *J. Appl. Phys.* **2003**, 93, 4485.